The Meteoritical Society

Meteoritics & Planetary Science 41, Nr 12, 1839–1852 (2006)
Abstract available online at http://meteoritics.org

Olivine zoning and retrograde olivine-orthopyroxene-metal equilibration in H5 and H6 chondrites

R. J. REISENER[1*], J. I. GOLDSTEIN[1], and M. I. PETAEV[2]

[1]Department of Mechanical and Industrial Engineering and Department of Geosciences, University of Massachusetts, Amherst, Massachusetts 01003, USA
[2]Harvard-Smithsonian Center for Astrophysics and Department of Earth and Planetary Sciences, Harvard University, Cambridge, Massachusetts 02138, USA
[*]Corresponding author. E-mail: reisener@mail.com

(Received 10 October 2005; revision accepted 05 September 2006)

Abstract–Electron microprobe studies of several H5 and H6 chondrites reveal that olivine crystals exhibit systematic Fe-Mg zoning near olivine-metal interfaces. Olivine Fa concentrations decrease by up to 2 mol% toward zoned taenite + kamacite particles (formed after relatively small amounts of taenite undercooling) and increase by up to 2 mol% toward zoneless plessite particles (formed after ~200 °C of taenite undercooling).

The olivine zoning can be understood in terms of localized olivine-orthopyroxene-metal reactions during cooling from the peak metamorphic temperature. The silicate-metal reactions were influenced by solid-state metal phase transformations, and the two types of olivine zoning profiles resulted from variable amounts of taenite undercooling at temperatures <700 °C. The relevant silicate-metal reactions are modeled using chemical thermodynamics.

Systematic olivine Fe-Mg zoning adjacent to metal is an expected consequence of retrograde silicate-metal reactions, and the presence of such zoning provides strong evidence that the silicate and metallic minerals evolved in situ during cooling from the peak metamorphic temperature.

INTRODUCTION

Ordinary chondrites contain 35–50 wt% olivine, ~30 wt% pyroxene, and 5–20 wt% Fe-Ni metal. In 1916, G. T. Prior observed that important relationships exist between the silicate and metallic minerals in chondrites: "the less the amount of nickel-iron in chondritic stones, the richer it is in nickel and the richer in iron are the magnesium silicates" (Prior 1916). Prior's Rules, which can be understood in terms of a redox-controlled distribution of Fe among olivine, pyroxene, and metal, illustrate that the silicate and metallic minerals interacted in order to approach or attain chemical equilibrium.

Most studies of olivine-orthopyroxene-metal equilibration in chondrites assume that the olivine and pyroxene compositions were established at the peak metamorphic temperature where high diffusion rates promote equilibration (Larimer 1968; McSween and Labotka 1993). According to Keil and Fredrickson (1964), Dodd (1969), Van Schmus and Wood (1967), Olsen and Bunch (1984), and Miyamoto et al. (1986), olivine crystals in types 4–6 ordinary chondrites are thought to be compositionally homogeneous. This result suggests that 1) olivine-orthopyroxene-metal equilibration was complete at the peak metamorphic temperature and 2) retrograde reactions among these minerals were insignificant. However, previous researchers did not investigate the possibility of systematic rim-to-core olivine Fe-Mg zoning that may have formed during slow cooling.

Several workers have attempted to quantify aspects of olivine-orthopyroxene-metal equilibria in chondrites. Mueller (1963) and Mueller and Olsen (1967) derived the mass balance equations that describe how olivine, orthopyroxene, and metal compositions and modes vary during isothermal redox reactions. Other workers used chemical thermodynamics to investigate the temperatures, pressures, and oxygen fugacities that prevailed during chondrite formation. Craig (1964) attempted to calculate chondrite equilibration temperatures on the basis of Fe-Mg partitioning between olivine and orthopyroxene. Mueller (1964), Larimer (1968), and Williams (1971) calculated chondrite equilibration temperatures and oxygen fugacities on the basis of the Fe distribution among olivine, orthopyroxene, and metal. Finally, McSween and Labotka (1993) calculated chondrite oxygen fugacities from olivine, orthopyroxene, and

© The Meteoritical Society, 2006. Printed in USA.

metal compositions. None of these studies, however, considered the effect of olivine-orthopyroxene-metal equilibration during cooling from the peak metamorphic temperature.

Van Schmus and Koffman (1967) recognized that chondrite orthopyroxene-diopside Fe-Mg exchange temperatures might reflect closure temperatures during cooling rather than peak metamorphic temperatures. More dramatically, chemical zoning in taenite (γ, face-centered-cubic) and kamacite (α, body-centered-cubic) are the result of taenite-kamacite equilibration during cooling (Wood 1967). It seems reasonable to expect, by analogy, that some degree of retrograde olivine-orthopyroxene-metal equilibration occurred.

The present study investigates the importance of olivine-orthopyroxene-metal equilibration in several H5 and H6 chondrites during cooling from the peak metamorphic temperature. These chondrites experienced metamorphic temperatures and time scales that were sufficient to homogenize individual olivine crystals (Miyamoto et al. 1986). Therefore, any systematic olivine zoning observed in these samples must have developed during cooling from the peak temperature. This study focuses on H-group chondrites because they are metal-rich and consequently contain a high density of silicate-metal interfaces where silicate zoning (resulting from silicate-metal reaction) might occur. Olivine and orthopyroxene crystals are analyzed near olivine-orthopyroxene, olivine-metal, and orthopyroxene-metal interfaces in order to search for silicate zoning. Additionally, a chemical thermodynamic model is developed to investigate the effect of taenite transformations (i.e., changing taenite compositions) on the equilibrium olivine and orthopyroxene compositions during cooling. This study represents the first attempt to investigate the importance of retrograde olivine-orthopyroxene-metal equilibration in chondrites.

BACKGROUND: TAENITE TRANSFORMATIONS DURING COOLING

In this paper, we demonstrate that silicate-metal reactions occurred in ordinary chondrites during cooling from the peak metamorphic temperature, and that these reactions were closely tied to the taenite transformations during cooling. Therefore it is important to review what is known about taenite transformations in ordinary chondrites.

There are two mechanisms by which taenite, which is stable at the peak metamorphic temperature, can transform to a more stable taenite + kamacite mixture upon cooling. In mechanism 1, taenite particles that are polycrystalline at high temperatures exsolve kamacite directly by the taenite $\rightarrow$ taenite + kamacite transformation; in mechanism 2, taenite particles that are monocrystalline at high temperatures decompose by the taenite $\rightarrow$ martensite $\rightarrow$ taenite + kamacite transformation (Reisener and Goldstein 2003a, 2003b). The two fundamentally different reaction paths for taenite decomposition are summarized below.

Polycrystalline Taenite: The Equilibrium Taenite Path

Consider the behavior of a parent taenite particle that is polycrystalline and contains 10 wt% Ni, a typical composition for metal particles in H chondrites (Fig. 1a). The taenite particle will cool below the taenite/(taenite + kamacite) solvus at ~700 °C (Fig. 1a). Kamacite will precipitate heterogeneously along internal taenite grain boundaries after relatively small amounts of undercooling below the solvus (Fig. 1b, left) (Reisener and Goldstein 2003a, 2003b). The grain boundary kamacite precipitate will grow by consuming one of the adjacent taenite grains (Reisener and Goldstein 2003b).

Initially, taenite and kamacite volume diffusion rates are sufficiently high that total taenite-kamacite equilibrium is maintained, i.e., taenite and kamacite remain homogeneous with compositions defined by the Fe-Ni phase diagram equilibrium tie-lines. However, volume diffusion rates decrease exponentially during cooling and mass transfer eventually becomes too sluggish to maintain total equilibrium. The classic M-shaped Ni profile develops in taenite and an Agrell Ni depletion develops in kamacite (Fig. 2b). Local equilibrium is maintained at the taenite/kamacite interface throughout the cooling process, even though taenite and kamacite do not maintain total equilibrium (Fig. 2b). Taenite-kamacite equilibrium is also maintained locally at taenite/silicate and kamacite/silicate interfaces (Fig. 2b) because Fe and Ni atoms diffuse across taenite and kamacite surfaces much faster than they diffuse through the taenite and kamacite lattices (Willis and Goldstein 1983).

The equilibrium taenite composition, γ_E, at taenite/kamacite and taenite/silicate interfaces follows the "equilibrium taenite path" during cooling (Fig. 1a, line A-E). The final metal microstructure formed from a polycrystalline taenite particle is a "zoned taenite + kamacite particle" such as the one shown on the left in Fig. 2a. At temperatures <500 °C, the taenite interior further decomposes by a variety of complex solid-state transformations (Yang et al. 1997).

Zoned taenite and kamacite frequently appear isolated from each other when viewed on the plane of sectioning. Sequential polishing, however, has shown that zoned taenite and kamacite are always connected to each other in the third dimension (Willis and Goldstein 1983).

Monocrystalline Taenite: The Metastable Taenite Path

Many parent taenite particles in type 5 and 6 ordinary chondrites were monocrystalline at the beginning of cooling due to the effect of taenite grain growth at high temperatures.

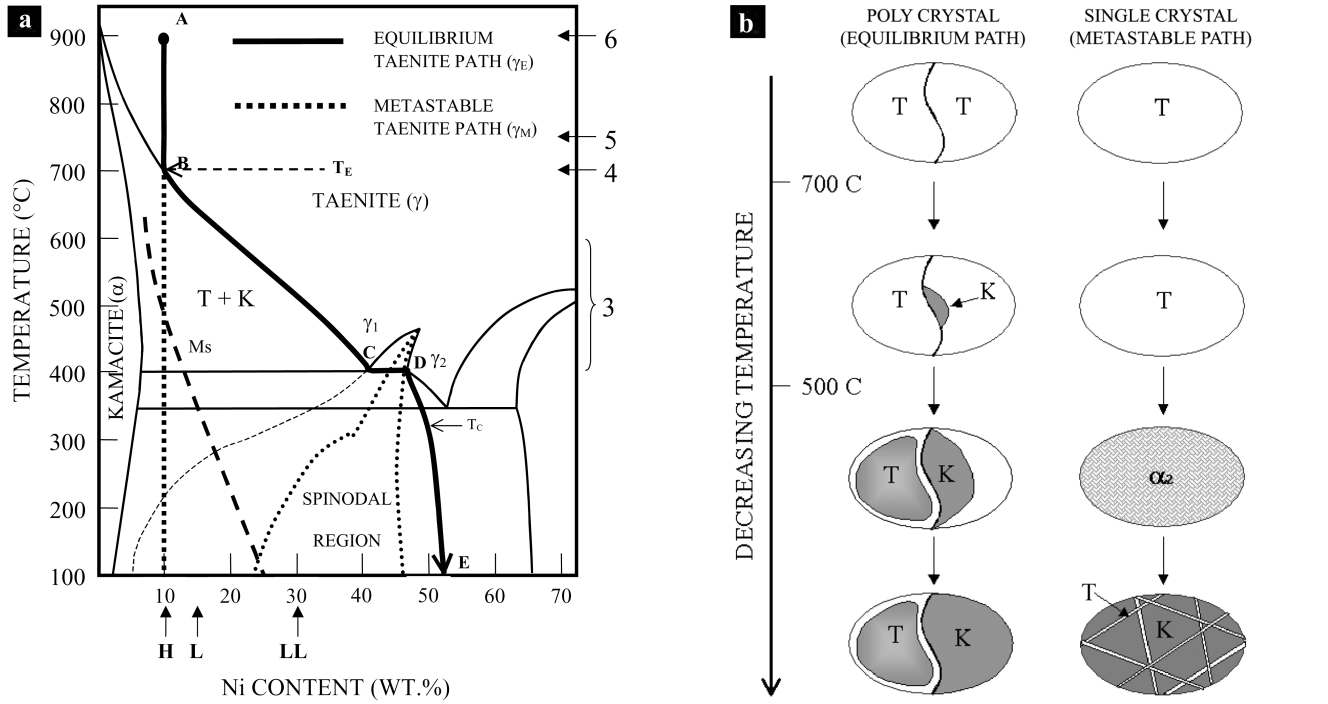

Fig. 1. a) Fe-Ni diagram showing taenite, kamacite, and taenite + kamacite (T + K) stability fields. Ms represents the martensite-start line. Line A → E indicates the equilibrium taenite path (γ_E) for an alloy of 10 wt% Ni. The vertical broken line indicates the metastable taenite path (γ_M). The peak temperatures reached by type 3 → 6 ordinary chondrites are indicated on the right, and the average metal Ni concentrations of H, L, and LL chondrites are indicated on the bottom. b) Evolution of polycrystalline taenite (left) and monocrystalline taenite (right) during cooling. T, K, and α_2 represent taenite, kamacite, and martensite, respectively.

A taenite particle that is monocrystalline will experience large amounts of undercooling because taenite/taenite boundaries, which serve as kamacite nucleation sites, are not present (Fig. 1b, right) (Reisener and Goldstein 2003a, 2003b). The undercooled taenite particle remains homogeneous and metastable (Fe-supersaturated at 10 wt% Ni) as it cools through the taenite + kamacite field (the metastable taenite composition, γ_M, is indicated by a vertical broken line in Fig. 1a). At ~500 °C (after ~200 °C of undercooling) the homogeneous taenite particle will cool below the martensite-start temperature (Fig. 1a, dashed line) and will transform to martensite (α_2, strained bcc) by the diffusionless taenite → martensite transformation (Fig. 1b). The homogeneous martensite, itself metastable, will subsequently decompose by the martensite → taenite + kamacite reaction during continued cooling (Fig. 1b). The final microstructure of the undercooled taenite particle is a two-phase, micron-scale mixture of taenite and kamacite known as plessite (Fig. 2a, right). These metal particles are named "zoneless plessite particles" because they lack systematic rim-to-core Ni zoning (Fig. 2b) (Sears and Axon 1975; Reisener and Goldstein 2003b).

In many well-equilibrated (type 5 and 6) ordinary chondrites, zoned taenite + kamacite particles and zoneless plessite particles coexist within microscopic distances of each other (Fig. 2a). Both types of metal particles had identical starting compositions and experienced the same cooling history, but the different parent taenite structures (polycrystalline versus monocrystalline) initiated different types of phase transformations resulting in different final metal microstructures (zoned taenite + kamacite particles versus zoneless plessite particles).

PROCEDURE

Polished thin sections of four low-shock (S1–S2), type 5–6 H-group chondrites were selected for detailed studies of olivine and orthopyroxene zoning: Estacado (H6), Guarena (H6), Kernouve (H6), and Nuevo Mercurio (H5). The four chondrites have well-recrystallized textures and coherent metallographic cooling rates indicating that they did not experience brecciation after cooling from the peak metamorphic temperature. Each chondrite contains two types of Fe-Ni metal particles: 1) zoned taenite + kamacite particles that formed after small amounts of taenite undercooling, and 2) zoneless plessite particles that formed after monocrystalline taenite undercooled ~200 °C below the taenite/(taenite + kamacite) solvus, as described by Reisener and Goldstein (2003a, 2003b).

The thin sections were polished with diamond paste from 15 μm down to 0.06 μm, and lightly etched with Nital (2 vol% HNO_3, balance ethyl alcohol) in order to reveal the fine-scale

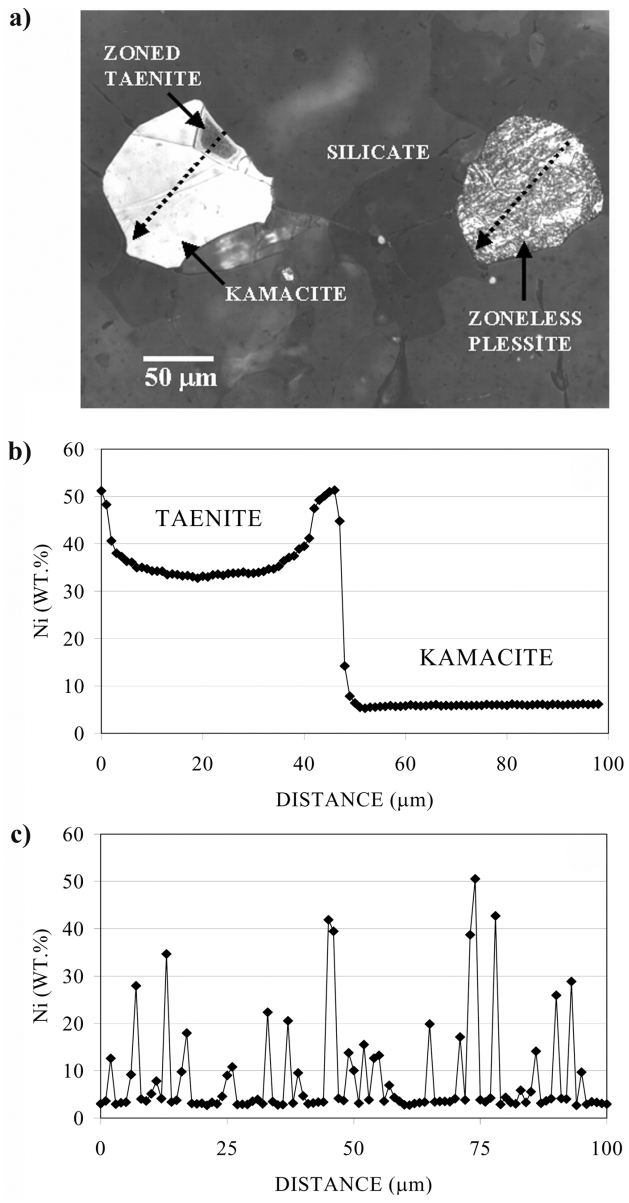

Fig. 2. a) An optical micrograph of Guarena (H6) showing a zoned taenite + kamacite particle (left) and a zoneless plessite particle (right). The broken lines indicate the approximate positions of electron microprobe line scans. b) Ni line scan across the zoned taenite + kamacite particle. The different zoned taenite sizes in (a) and (b) reflect migration of the taenite/kamacite interface during repeated polishing. c) Ni line scan across the zoneless plessite particle.

metal microstructures. Reflected-light microscopy was used to classify each metal particle as a zoned taenite + kamacite particle or as a zoneless plessite particle (Fig. 2a). The petrographic settings of olivine and orthopyroxene crystals were classified into one of three categories: 1) crystals that are isolated from Fe-Ni metal (surrounded by other silicate crystals), 2) crystals that abut zoned taenite + kamacite particles, and 3) crystals that abut zoneless plessite particles.

A Cameca SX50 electron microprobe, operated at an accelerating voltage of 15 kV and a beam current of 20 nA, was used to analyze Si, Fe, Mg, Mn, Ca, Ni, Cr, and Al in olivine and orthopyroxene crystals using a 40-second counting time for each element. These conditions gave a one standard deviation uncertainty of <0.1 wt% for SiO_2, FeO, and MgO. The microprobe standards were synthetic fayalite (for Fe and Si), Shallowater enstatite (Mg), Broken Hill rhodonite (Mn), Kiglapait labradorite (Ca and Al), synthetic NiO (Ni), and Stillwater chromite (Cr). Quantitative analyses were obtained using the PAP φ(ρz) routine.

Silicate-metal interfaces were studied using both reflected-light and transmitted-light microscopy. The positions of silicate-metal interfaces, as viewed in reflected light, often shift toward the silicate when viewed in transmitted light. This optical effect indicates that an opaque mineral such as metal or troilite underlies silicate below the plane of sectioning. Electron microprobe analyses were collected only from olivine and orthopyroxene crystals that do not overlie opaque minerals, minimizing the possibility that Fe X-rays were generated by subsurface metal or troilite.

Olivine and orthopyroxene crystals were analyzed using line scans (1 μm step intervals) across olivine-orthopyroxene interfaces, olivine-metal interfaces, and orthopyroxene-metal interfaces. Additionally, point analyses were obtained at olivine cores and at olivine rims (including olivine-metal interfaces) in order to rapidly characterize compositional zoning patterns in olivine.

RESULTS

Silicate Crystals Isolated from Fe-Ni Metal

Individual olivine and orthopyroxene crystals that are isolated from metal have core and rim compositions that are identical within analytical uncertainties. However, silicate compositions vary by up to ~1 mol% Fa or Fs from one crystal to another in each chondrite. Figure 3 shows fayalite measurements in olivine crystals that are isolated from metal in the four H chondrites (the analyses are represented by circles).

Electron microprobe line scans collected across olivine-orthopyroxene interfaces in Estacado (H6) and Kernouve (H6) are shown in Fig. 4. No systematic FeO/(FeO + MgO) zoning was observed at the interfaces. In each chondrite, olivine Fa concentrations are higher than orthopyroxene Fs concentrations (Fig. 4). The measured distribution of Fe and Mg between olivine and orthopyroxene is consistent with the work of Keil et al. (1964) and Larimer (1968) and also is consistent with experimental FeO-MgO-SiO_2 system equilibria (Larimer 1968).

In addition to the major elements, olivine contains 0.4–0.6 wt% MnO and 0.01–0.05 wt% Ca; orthopyroxene contains 0.5–0.6 wt% MnO and ~0.6 wt% CaO.

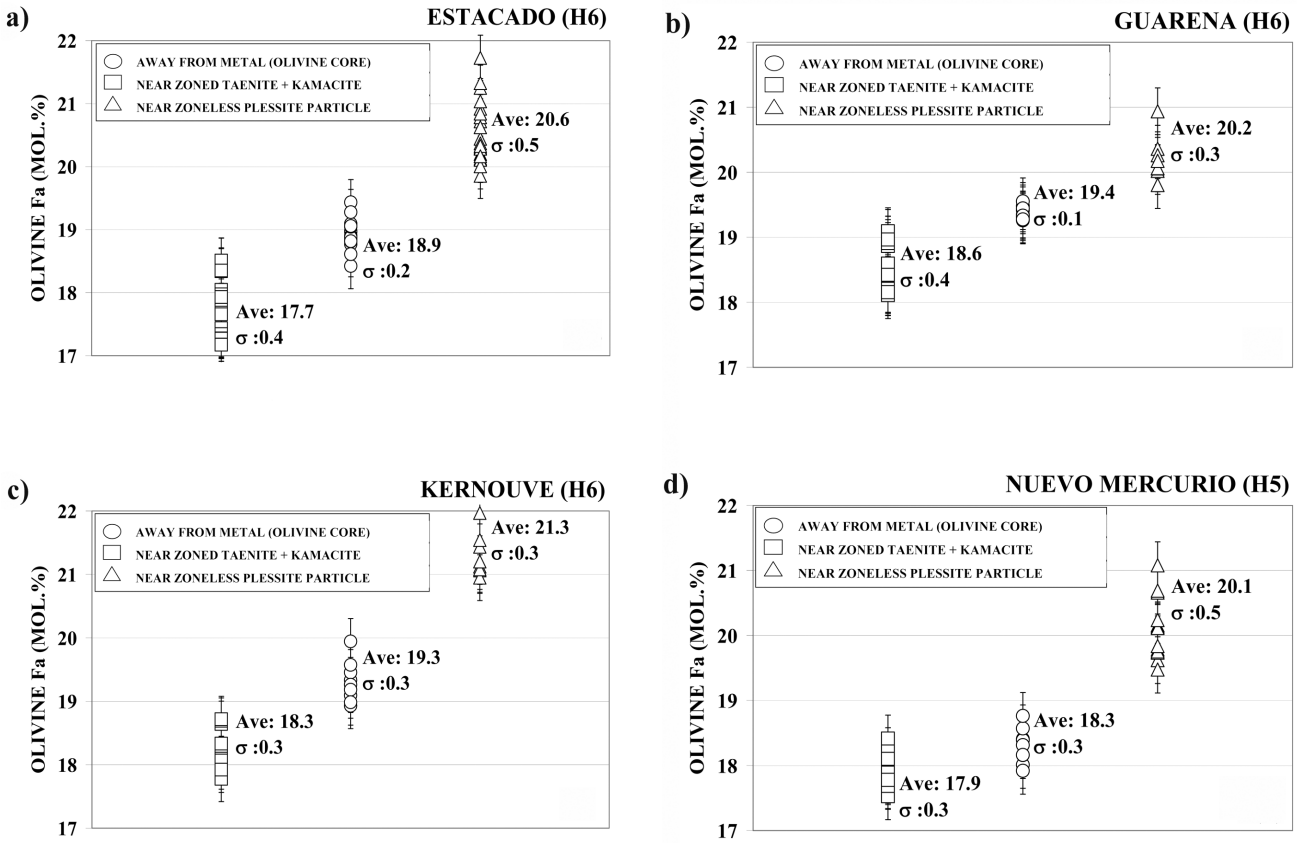

Fig. 3. Figures 3a–d report electron microprobe analyses of olivine crystals in different petrographic settings. Squares represent analyses collected within 10 μm of zoned taenite + kamacite particles. Triangles represent analyses collected within 10 μm of zoneless plessite particles. Circles represent analyses collected at the cores of olivine crystals that are isolated from Fe-Ni metal. Each data point represents a single analysis collected on a unique olivine crystal. Error bars represent the 2σ uncertainty level.

Silicate Crystals Abutting Zoned Taenite + Kamacite Particles

Electron microprobe line scans, traversing olivine crystals toward zoned taenite + kamacite particles, are reported as squares in Fig. 5. Olivine Fa concentrations decrease systematically by ~2 mol% as a zoned taenite + kamacite particle is approached. The zoning extends 30–40 μm from the metal, and is independent of whether the olivine abuts zoned taenite or the coexisting kamacite. An olivine Fa concentration decrease is also shown in Fig. 3, in which analyses collected within 10 μm of a zoned taenite + kamacite particle are reported as squares. In contrast to the FeO depletion in olivine, MnO concentrations are homogeneous. Our electron microprobe data show that orthopyroxene Fs concentrations remain constant as zoned taenite + kamacite particles are approached.

Silicate Crystals Abutting Zoneless Plessite Particles

Electron microprobe line scans, traversing olivine crystals toward zoneless plessite particles, are reported as triangles in Fig. 5. Olivine Fa concentrations increase systematically by ~2 mol% as a zoneless plessite particle is approached; the zoning extends 30–40 μm from the metal. An olivine Fa concentration increase is also shown in Fig. 3, in which analyses collected within 10 μm of a zoneless plessite particle are reported as triangles. MnO concentrations are homogeneous along the Fe-Mg zoning profiles. Orthopyroxene Fs concentrations appear to remain constant as zoneless plessite particles are approached.

Olivine Stoichiometry

Olivine and orthopyroxene crystals in all three textural settings are stoichiometric with respect to SiO_2, FeO, MgO, and MnO. Cation totals in olivine are 3.00 ± 0.05, even along the Fe-Mg zoning profiles.

DISCUSSION

Is the Olivine Zoning Real?

It is important to evaluate whether the observed olivine Fa variations could be artifacts of the electron probe

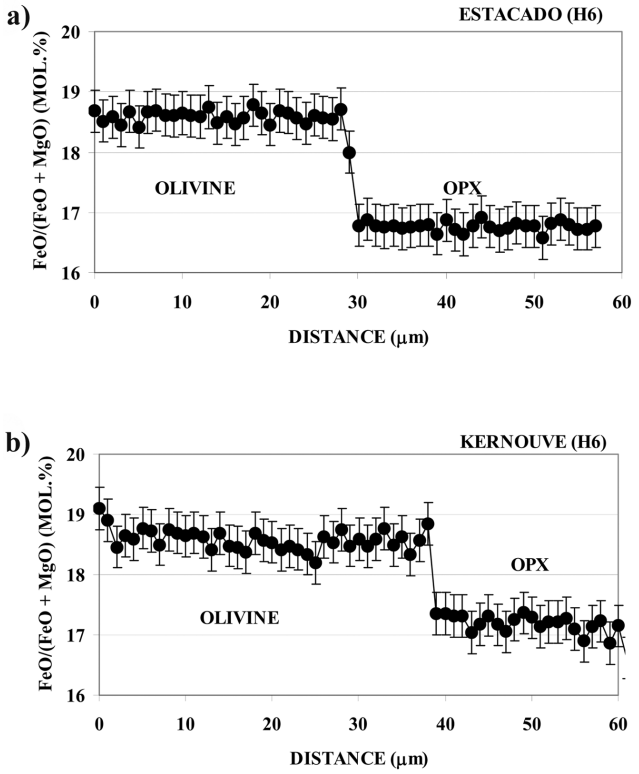

Fig. 4. (a) and (b) report electron microprobe line scans across olivine-orthopyroxene interfaces (the crystals are isolated from Fe-Ni metal). The olivine and orthopyroxene crystals are homogeneous within electron microprobe counting statistics.

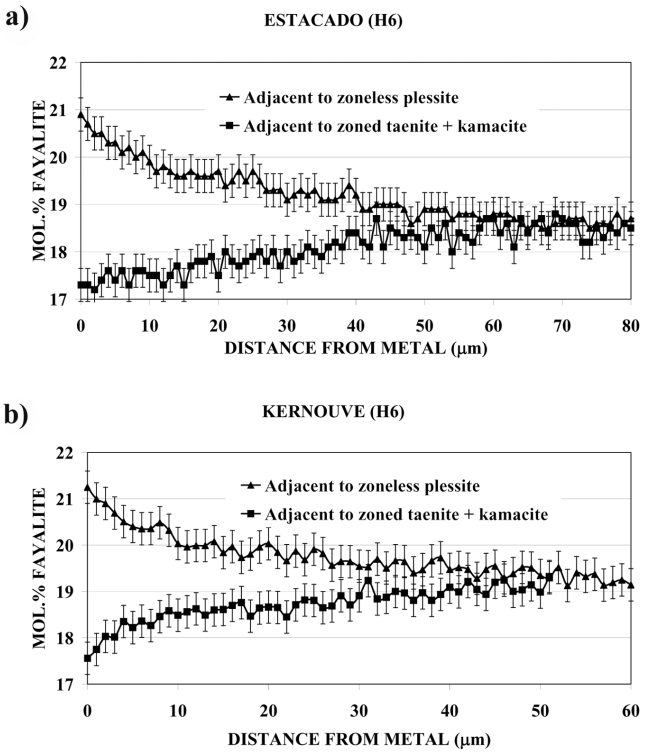

Fig. 5. (a) and (b) report olivine composition as a function of distance from Fe-Ni metal. Analyses represented by squares were collected while traversing olivine toward zoned taenite + kamacite particles; analyses represented by triangles were collected while traversing olivine toward zoneless plessite particles. Olivine-metal interfaces are positioned at the left (distance = 0 μm).

microanalysis. When an olivine crystal is analyzed near an olivine-metal interface, electron-sample interactions and X-ray fluorescence can potentially excite Fe atoms in the metal resulting in apparent Fa concentrations that are erroneously high. It is conceivable that electron-sample interactions and/or X-ray fluorescence could explain the elevated olivine Fa concentrations measured near zoneless plessite particles (neither effect, however, can explain the low olivine Fa concentrations measured near zoned taenite + kamacite particles). The potential effects of electron-sample interactions and X-ray fluorescence are evaluated below.

Electron-Sample Interactions: Primary X-ray Generation Volume

The spatial resolution of the electron microprobe is determined by the volume of primary X-ray generation. When the electron beam is situated in olivine near an olivine-metal interface, the volume of X-ray generation may potentially overlap metal resulting in Fa concentrations that are erroneously high.

The cross-sectional radius of the primary X-ray generation volume is given by the Kanaya-Okayama formula:

$$R = \frac{0.0276AE^{1.67}}{Z^{0.89}\rho} \quad (1)$$

where R is the electron range in microns, A is the sample's average molecular weight, E is the electron beam energy in kV, Z is the sample's average atomic number, and ρ is the sample's density in g/cm^3 (Goldstein et al. 1992). Using appropriate values for olivine (A ~20, Z ~10, and ρ ~3.5) and an electron beam energy of 15 kV, the cross-sectional radius is calculated as 2–3 μm. The primary X-ray interaction volume, therefore, is too small to explain olivine Fa enrichments more than a few microns from zoneless plessite particles.

Characteristic X-ray Fluorescence

Characteristic X-rays traveling though a sample can ionize atoms resulting in the fluorescence of other X-rays. The volume of X-ray fluorescence is much larger than the volume of electron interaction because X-rays penetrate solids more efficiently than electrons. However, the characteristic X-rays generated by the major elements in olivine (Si, Fe, Mg, and Mn) have insufficient energy to excite Fe Kα radiation (7.11 keV) in the metal. Therefore, the

elevated olivine Fa concentrations measured near zoneless plessite particles cannot be explained by characteristic X-ray fluorescence.

Continuum X-ray Fluorescence

The background continuum radiation produced during electron probe microanalysis provides X-rays with energies ranging from 0 eV up to the electron beam energy. For the 15 keV beam used in this study, the continuum radiation is capable of exciting Fe X-rays (K edge = 7.11 keV) and Ni X-rays (K edge = 8.33 keV) in metal. However, less than 0.05 wt% Ni is measured during olivine analyses (even near olivine-metal interfaces). This result suggests, by analogy, that continuum fluorescence of metallic Fe does not make a significant contribution to the measured Fe intensities.

The importance of continuum fluorescence was also investigated experimentally. A piece of San Carlos olivine (Fo_{90}) and a piece of synthetic Fe-Ni alloy ($Fe_{10}Ni$) were clamped together along flat surfaces. An electron microprobe line scan (1 μm step interval) was used to measure the composition of olivine as the olivine-metal interface was approached. Olivine Fa concentrations were constant until the electron beam was within ~3 μm from the olivine-metal interface. Within 3 μm of the metal, olivine Fa concentrations increase by several mol% because the electron interaction volume overlaps the metal. This experiment confirms that X-ray fluorescence of metallic Fe cannot explain the elevated olivine Fa concentrations that extend up to 30 μm from zoneless plessite particles.

Olivine Stoichiometry

The measured stoichiometry of the olivine provides additional evidence that the Fe-Mg zoning is real. If the elevated olivine Fa concentrations measured near zoneless plessite particles were caused by electron-sample interactions or X-ray fluorescence, cation totals (Si + Fe + Mg + Mn) would exceed 3.0 due to Fe X-ray contributions from metal. Cation totals along the olivine Fe-Mg zoning profiles are 3.00 ± 0.05, indicating that negligible amounts of Fe X-rays were generated in the adjacent metal.

In summary, neither electron excitation nor X-ray fluorescence can explain the elevated olivine Fa concentrations measured near zoneless plessite particles. Moreover, neither of these effects can explain the low olivine Fa concentrations measured near zoned taenite + kamacite particles. The authors conclude that the systematic olivine Fe-Mg zoning measured near Fe-Ni metal particles is real.

Origin of Olivine Zoning by Solid-State Reaction

Two fundamentally different mechanisms can cause systematic Fe-Mg zoning in olivine: 1) nonequilibrium crystallization of olivine from a melt (igneous zoning) and 2) solid-state equilibration between olivine and other Fe-bearing minerals (metamorphic zoning). Igneous zoning in olivine is characterized by Fa concentrations that increase systematically from crystal core to crystal rim. Olivine crystals in type 3 ordinary chondrites display igneous zoning due to rapid chondrule solidification rates, but in type 5 and 6 chondrites such zoning would have been completely homogenized during metamorphism by solid-state diffusion (Miyamoto et al. 1986).

Olivine crystals in the H5 and H6 chondrites exhibit Fe-Mg zoning only where they abut Fe-Ni metal, suggesting an origin by silicate-metal reaction in the solid state. Moreover, the observation that olivine zoning profiles adjacent to zoned taenite + kamacite particles differ from olivine zoning profiles adjacent to zoneless plessite particles suggests that the zoning is linked to the metal transformation path, i.e., the olivine zoning developed during cooling from the peak metamorphic temperature.

The meteorite literature contains few reports of olivine zoning resulting from solid-state reactions between silicate and metal. In pallasites, consisting mainly of olivine crystals surrounded by metal, olivine exhibits slight Fe-Mg zoning from crystal core to rim (Miyamoto 1997). In Esquel and Yamato 8451 (a pyroxene-bearing pallasite) olivine Fa decreases by ~1 mol% from crystal core to rim. In Imilac, some olivine crystals show Fa-enrichment toward the rim while other olivine crystals show the opposite zoning pattern. Miyamoto (1997) did not discuss the origin of the pallasite olivine zoning profiles in detail, but he did entertain the possibility that the zoning formed during subsolidus cooling.

In another relevant study, Dohmen et al. (1998) addressed the formation of olivine FeO-enrichment halos around Fe-Ni metal inclusions in Allende (CV3). Experimental studies of the system olivine + metal led to the unexpected conclusion that Mg-rich olivine can react with metallic Fe, even in the absence of other Mg-bearing minerals that provide a sink for Mg transported away from the olivine-metal interface. The olivine-metal reaction is possible because Mg is lost from the interface via a gaseous phase.

As we shall see, olivine zoning may develop in chondrites by silicate-metal reaction without loss of Mg from the system. The experimental study by Dohmen et al. (1998) may be relevant, however, in explaining intergranular transport of chemical components within chondrites via a dry vapor phase composed of Fe, Mg, SiO, O_2, O, etc.

Silicate-Metal Equilibria: Thermodynamic Analysis

In this section, chemical thermodynamics will be used to investigate the compositional evolution of olivine + orthopyroxene + metal assemblages in ordinary chondrites during cooling from the peak metamorphic temperature. A new analysis of silicate-metal equilibration incorporates two

major effects that were neglected during previous studies: 1) taenite composition changes during cooling and 2) the tendency for many taenite particles to undercool within the taenite + kamacite field (i.e., the occurrence of equilibrium taenite and metastable taenite within the same chondrite).

Reactions

Chondritic olivine and orthopyroxene are essentially binary solutions of the Fe-Mg endmembers, fayalite-forsterite and ferrosilite-enstatite respectively. These silicates coexist with the Fe-Ni metal phases taenite and kamacite. Taenite is the stable metallic phase at temperatures above the taenite/(taenite + kamacite) solvus, while taenite and kamacite are in equilibrium at temperatures below the solvus. In addition, the oxygen fugacity (fO_2) plays an important role during silicate-metal equilibration.

Three reactions completely describe the equilibria among olivine, orthopyroxene, taenite, and kamacite:

$$\overset{\text{Olivine}}{Fe_2SiO_4} = \overset{\text{Orthopyroxene}}{FeSiO_3} + \overset{\text{Taenite}}{Fe} + \frac{1}{2}\overset{\text{Gas}}{O_2} \qquad \text{Reaction 1}$$

$$\overset{\text{Orthopyroxene}}{MgSiO_3} + \frac{1}{2}\overset{\text{Olivine}}{Fe_2SiO_4} = \overset{\text{Orthopyroxene}}{FeSiO_3} + \frac{1}{2}\overset{\text{Olivine}}{Mg_2SiO_4} \qquad \text{Reaction 2}$$

$$\overset{\text{Taenite}}{Fe} + \overset{\text{Kamacite}}{Ni} = \overset{\text{Taenite}}{Ni} + \overset{\text{Kamacite}}{Fe} \qquad \text{Reaction 3}$$

An increase in oxygen fugacity will drive Reaction 1 to the left producing olivine at the expense of orthopyroxene and metallic Fe (oxidation). Olivine becomes FeO-enriched as iron is transferred from metal to silicate, and the residual metal becomes Fe-depleted (relatively Ni-enriched). Simultaneously, equilibration between olivine and orthopyroxene (Reaction 2) will result in Fe-enrichment of orthopyroxene. Mass balance is maintained during oxidation via the partitioning of SiO_2 between orthopyroxene and olivine.

A decrease in oxygen fugacity (reduction) will drive Reaction 1 to the right producing orthopyroxene and metallic Fe at the expense of olivine; the olivine and orthopyroxene will become MgO-enriched and the metal will become Fe-enriched (relatively Ni-depleted). Partitioning of SiO_2 between olivine and orthopyroxene allows mass balance to be maintained during the reduction process.

It is important to note that analogous redox reactions can be driven by variations in taenite composition. At a given temperature and oxygen fugacity, an increase in taenite Fe concentration will drive Reaction 1 to the left (oxidation) while a decrease in taenite Fe concentration will drive the reaction to the right (reduction).

It should also be noted that Reaction 1 is written in terms of taenite rather than kamacite. This treatment is clearly valid at temperatures above the taenite/(taenite + kamacite) solvus because taenite is the only stable metallic phase. This approach is also justified at temperatures below the taenite/(taenite + kamacite) solvus because the reaction that describes taenite-kamacite equilibrium (Reaction 3) is independent of the reactions describing olivine-orthopyroxene-taenite equilibria (Reactions 1 and 2). At temperatures <700 °C, taenite-kamacite equilibrium forces the taenite composition to follow the taenite/(taenite + kamacite) solvus of the Fe-Ni phase diagram. Therefore, the equilibrium taenite and kamacite compositions can be obtained directly from the Fe-Ni phase diagram at any temperature.

Formalism

Olivine and orthopyroxene in equilibrated ordinary chondrites can be regarded as binary solutions of the Fe-Mg endmembers. In reality, olivine contains 0.4–0.6 wt% MnO and less than 0.1 wt% CaO and orthopyroxene contains 0.4–0.6 wt% MnO and 0.5–1 wt% CaO. The low concentrations of MnO and CaO, however, should have little influence on Reactions 1 or 2. Indeed, there is close experimental agreement between Fe-Mg partitioning studies in which olivine and orthopyroxene are Ca-free and Fe-Mg partitioning studies in which olivine and orthopyroxene contain up to 1.0 wt% Ca (Larimer 1968).

Using the ionic solution model (e.g., Ganguly and Saxena 1987) the activity, a, of an end-member component in a phase m with a general formula $(i, j, \ldots)_\alpha Q$ can be expressed as:

$$a^m_{i_\alpha Q} = (\chi^m_i \cdot \lambda^m_i)^\alpha \qquad (2)$$

Here χ is the component's molecular concentration, λ is the component's activity coefficient, and α represents the number of different crystallographic mixing sites in the mineral. The value of α for taenite and orthopyroxene is 1; for olivine, the value is 2. The activity coefficients of fayalite, forsterite, ferrosilite, and enstatite are approximated by the symmetrical solution model (Ganguly and Saxena 1987):

$$\lambda^m_i = \exp\left[\frac{(1-\chi^m_i)^2 W^M_{\text{Fe}-\text{Mg}}}{\alpha RT}\right] \qquad (3)$$

where T is the temperature, R is the gas constant, and $W_{\text{Fe-Mg}}$ is the Fe-Mg interaction parameter for olivine or orthopyroxene (Berman and Aranovich 1996). The activity coefficient of Fe in taenite is approximated by the subregular asymmetrical solution model:

$$\lambda_{\text{Fe}} = \exp\left[\frac{x^2_{\text{Ni}}[W_{\text{FeNi}} + 2(W_{\text{FeNi}} - W_{\text{FeNi}})x_{\text{Fe}}]}{\alpha RT}\right] \qquad (4)$$

where W_{FeNi} and W_{NiFe} are the Fe-Ni interaction parameters (Hsieh et al. 1987).

The equilibrium constants for Reactions 1 and 2 are:

$$K_1 = \frac{(fO_2)^{1/2}(\chi_{Fe}^{Taenite} \cdot \lambda_{Fe}^{Taenite})(\chi_{Fe}^{OPX} \cdot \lambda_{Fe}^{OPX})}{(\chi_{Fe}^{Olivine} \cdot \lambda_{Fe}^{Olivine})^2} \quad (5)$$

and

$$K_2 = \frac{(\chi_{Mg}^{Olivine} \cdot \lambda_{Mg}^{Olivine})(\chi_{Fe}^{OPX} \cdot \lambda_{Fe}^{OPX})}{(\chi_{Fe}^{Olivine} \cdot \lambda_{Fe}^{Olivine})(\chi_{Mg}^{OPX} \cdot \lambda_{Mg}^{OPX})} \quad (6)$$

Reactions 1 and 2 are related to their respective equilibrium constants by the law of mass action:

$$\Delta G_{rxn1,\,T} = -RT\ln K_1 \quad (7)$$

and

$$\Delta G_{rxn2,\,T} = -RT\ln K_2 \quad (8)$$

where ΔG is the Gibbs free energy change of the reaction.

For each reaction, the Gibbs free energy change can be calculated from the Gibbs free energies of formation of the individual mineral components:

$$\Delta G_{rxn,\,T} = \Sigma_{\nu_i}\Delta G_{f,\,T(\text{products})} - \Sigma_{\nu_i}\Delta G_{f,\,T(\text{reactants})} \quad (9)$$

where v_i are the stoichiometry coefficients. The standard Gibbs free energy of formation of each mineral component is given by:

$$\Delta G_{f,\,T} = \Delta H^{\circ}_{f,\,298.15} - T \cdot S^{\circ}_{298.15} + \int_{298.15}^{T} Cp\,dT - T \cdot \int_{298.15}^{T} \frac{Cp}{T}\,dT \quad (10)$$

where $\Delta H^{\circ}_{f,\,298.15}$ and $S^{\circ}_{298.15}$ represent the standard enthalpy of formation from elements and standard entropy (respectively) of a mineral component at 298 K and 1 bar, and *Cp* represents the heat capacity of the mineral component. No pressure correction is included in Equation 10 because pressure has little effect on Reactions 1 or 2 at lithostatic pressures below several kilobars (Larimer 1968). The standard thermodynamic properties of the silicate minerals are from Berman and Aranovich (1996), and those of oxygen and metallic Fe are from Chase (1998).

Calculations

The compositions of olivine and orthopyroxene in equilibrium with Fe-Ni metal during cooling can be calculated using chemical thermodynamics. Such calculations will be used to trace the silicate compositions from an assumed peak metamorphic temperature of 900 °C to a final temperature of 500 °C (a temperature below typical silicate closure temperatures). Three assumptions are made: 1) olivine, orthopyroxene, and taenite are fully equilibrated (hence homogeneous) at the onset of cooling; 2) all parent taenite particles have bulk compositions of 10 wt% Ni, typical of metal particles in H chondrites (Fig. 1a); and 3) the oxygen fugacity is defined by olivine-orthopyroxene-metal equilibria and is homogeneous throughout the chondrite at all times.

Olivine and Orthopyroxene Compositions at the Peak Metamorphic Temperature (900 °C)

Geothermometry shows that type 6 ordinary chondrites reached a peak metamorphic temperature of 750–950 °C (Dodd 1981). The compositions of olivine and orthopyroxene at an assumed peak temperature of 900 °C can be estimated from measured compositions and thermodynamic data. Figure 6 shows the equilibrium Fe-Mg distribution between olivine and orthopyroxene, calculated by simultaneously solving Equations 3, 6, 8, 9, and 10. The closure temperature for olivine-orthopyroxene Fe-Mg exchange in Estacado (H6) and Kernouve (H6) can be estimated from the compositions of coexisting crystals of olivine and orthopyroxene shown in Fig. 4 (these crystals are isolated from metal and hence homogeneous within microprobe counting statistics). In both chondrites, the olivine composition is ~18.5 Fa and the orthopyroxene composition is ~17.0 Fs, suggesting a final equilibration temperature of ~600 °C (Fig. 6). The olivine and orthopyroxene compositions at 900 °C can be found by extrapolation of the measured compositions (Fig. 4) to the 900 °C isotherm in Fig. 6 (mass conservation constrains the olivine and orthopyroxene compositions to a line of slope = –1). The extrapolation yields an olivine composition of ~19.0 Fa and an orthopyroxene composition of ~16.5 Fs at 900 °C.

The "Chondritic fO_2-T Path"

Before calculating equilibrium olivine and orthopyroxene compositions as a function of temperature, it is necessary to derive the relationship among chondrite oxygen fugacity, mineral compositions, and temperature. By rearranging Equation 5, the oxygen fugacity of an olivine + orthopyroxene + taenite assemblage at a given temperature can be expressed as:

$$\log fO_2 = 2\left\{\log K_1 - \log\left[\frac{(\chi_{Fe}^{Taenite}\lambda_{Fe}^{Taenite})(\chi_{Fe}^{OPX}\lambda_{Fe}^{OPX})}{(\chi_{Fe}^{Olivine}\lambda_{Fe}^{Olivine})^2}\right]\right\} \quad (11)$$

fO_2-T Relations between 900 and 700 °C: As olivine + orthopyroxene + taenite assemblages cool from 900 to 700 °C, each taenite particle contains 10 wt% Ni (Fig. 1a) and remains chemically homogeneous throughout cooling. However, the compositions of both olivine and orthopyroxene

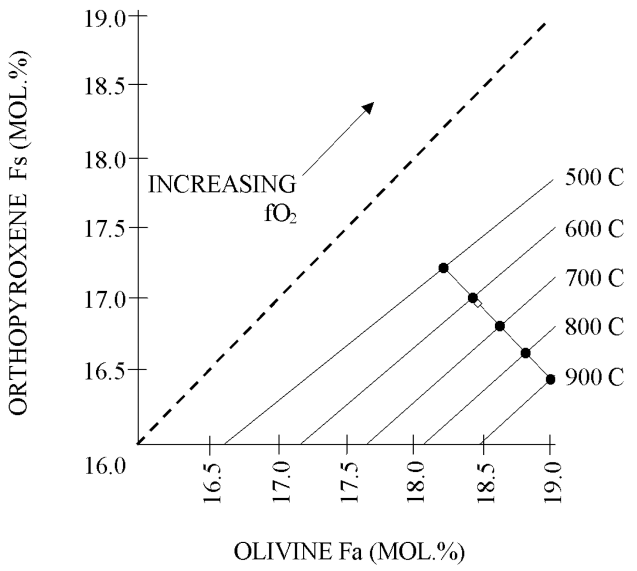

Fig. 6. Compositions of coexisting olivine and orthopyroxene between 900 and 500 °C due to Fe-Mg exchange (Reaction 2). The open diamond represents the compositions of coexisting olivine and orthopyroxene measured in this study. The dots trace the compositional evolution of the olivine + orthopyroxene pair between 900 and 500 °C. Mass conservation during Fe-Mg exchange constrains the silicate compositions to a slope of −1. The dashed line represents the condition that olivine Fa = orthopyroxene Fs.

change with temperature due to Fe-Mg exchange equilibrium. The oxygen fugacity defined by the olivine + orthopyroxene + taenite assemblage over this temperature range is calculated by solving Equations 3–11 simultaneously. Only one taenite composition is present over this temperature interval and therefore a single fO_2-T path is generated during cooling.

fO_2-T Relations between 700 and 500 °C: At temperatures <700 °C, taenite particles that are polycrystalline will precipitate kamacite at taenite/taenite boundaries while taenite particles that are monocrystalline will undercool without forming kamacite. The two different metal reaction paths produce two populations of taenite compositions: polycrystalline taenite will have the equilibrium taenite composition, γ_E, defined by the Fe-Ni phase diagram (Fig. 1a) whereas monocrystalline taenite will retain the metastable composition (γ_M) of ~10 wt% Ni throughout cooling.

Clearly, whole-rock silicate-metal equilibrium is not possible in the presence of two populations of taenite compositions (γ_E and γ_M) (Fig. 1a). Olivine, orthopyroxene, and taenite can establish local equilibria, however, either by adjustments in the local oxygen fugacity or by exchange of Fe between metal and silicates.

Assuming that the oxygen fugacity is defined by olivine-orthopyroxene-taenite equilibria, the two populations of taenite compositions will produce two fO_2-T paths at temperatures <700 °C. The fO_2-T path defined by an ol + opx + γ_E assemblage can be calculated using the olivine and orthopyroxene compositions in Fig. 6 (dots) and taenite compositions along the equilibrium taenite path in Fig. 1a. Similarly, the fO_2-T path defined by an ol + opx + γ_M assemblage can be calculated using the silicate compositions in Fig. 6 (dots) and a constant taenite composition of 10 wt% Ni (equilibrium is assumed to exist between metastable taenite, olivine, and orthopyroxene). Calculations for the 700 to 500 °C temperature interval show that the oxygen fugacity defined by an ol + opx + γ_E assemblage is up to 0.1 log unit higher than the oxygen fugacity defined by an ol + opx + γ_M assemblage. The two fO_2-T paths diverge during cooling because the equilibrium taenite and metastable taenite compositions diverge as temperature decreases (Fig. 1a).

The existence of two different fO_2-T paths within the same chondrite is inherently unstable and some degree of oxygen fugacity homogenization will occur. Oxygen fugacity homogenization will be promoted by the slow cooling rates of ordinary chondrites (typically on the order of 1–100 °C/MY; Wood 1967; Pellas and Storzer 1981; Willis and Goldstein 1983) and high chondrite permeabilities (Sugiura et al. 1986). A "chondritic fO_2-T path," representing the whole-rock oxygen fugacity after homogenization, can be approximated by averaging the fO_2-T path defined by an ol + opx + γ_E assemblage and the fO_2-T path defined by an ol + opx + γ_M assemblage. The resulting fO_2-T path is shown as a solid line in Fig. 7a. The ferrosilite-iron-fayalite (FIF) buffer and the intrinsic oxygen fugacities measured in H chondrites (Brett and Sato 1984) are plotted in the same figure for reference. The chondritic fO_2-T path calculated in the present study is lower than the intrinsic oxygen fugacity path, but the calculated fO_2-T path is consistent with H chondrite oxygen fugacities calculated by McSween and Labotka (1993) on the basis of mineral compositions. The intrinsic oxygen fugacities measured by Brett and Sato (1984) lie above the FIF buffer at temperatures <750 °C and consequently are incompatible with ordinary chondrite mineralogy. As explained below, we propose that it is the chondritic (homogenized) oxygen fugacity that drives redox reactions at silicate-metal interfaces.

Olivine and Orthopyroxene Compositions During Cooling

As an olivine + orthopyroxene + taenite assemblage cools, the olivine and orthopyroxene compositions will vary due to the combined effects of redox and Fe-Mg exchange equilibria (Reactions 1 and 2). The compositions of olivine and orthopyroxene in equilibrium with metal can be calculated by simultaneously solving Equations 3–10 for the 900–500 °C temperature interval. Specifically, the silicate compositions coexisting with equilibrium taenite (γ_E) can be calculated using taenite compositions along the equilibrium taenite path (Fig. 1a) and oxygen fugacities along the chondritic fO_2-T path shown in Fig. 7. Similarly, the silicate compositions coexisting with metastable taenite (γ_M) can be

calculated using a constant taenite composition of 10 wt% Ni and oxygen fugacities along the chondritic fO_2-T path (Fig. 7). The calculated silicate compositions in ol + opx + γ_E assemblages are reported as solid lines in Fig. 8. The calculated silicate compositions in ol + opx + γ_M assemblages are reported as broken lines in the same figure.

Cooling from 900 to 700 °C: Olivine and orthopyroxene will have initial (900 °C) compositions of 19.0 Fa and 16.5 Fs respectively. As olivine + orthopyroxene + taenite assemblages cool to the taenite/(taenite + kamacite) solvus at 700 °C, all taenite particles remain homogeneous at 10 wt% Ni (Fig. 1a). The oxygen fugacity (defined by olivine + orthopyroxene + taenite equilibria) is constant everywhere within the chondrite. During cooling, olivine Fa concentrations decrease slightly and orthopyroxene Fs concentrations increase slightly (Fig. 8) due to Fe-Mg exchange (Reaction 2).

Cooling from 700 to 500 °C: At 700 °C, the taenite particles cool into the two-phase taenite + kamacite field (Fig. 1a). If a parent taenite particle is polycrystalline, kamacite will precipitate at the taenite/taenite grain boundaries by the reaction taenite → taenite + kamacite (Fig. 1b). The equilibrium Ni concentration in taenite (γ_E) at the taenite/silicate interface increases along the equilibrium taenite path throughout cooling (Fig. 1a).

If a parent taenite particle is monocrystalline, it will undercool below the taenite/(taenite + kamacite) solvus without forming kamacite. The composition of the metastable taenite (γ_M) at the taenite/silicate interface will remain constant at ~10 wt% Ni throughout cooling (Fig. 1b) (Reisener and Goldstein 2003b). The compositions of γ_E and γ_M at taenite/silicate interfaces will diverge along the γ_E and γ_M paths throughout cooling (Fig. 1a).

From 700 to 500 °C, olivine and orthopyroxene compositions change dramatically (Fig. 8) due to the effect of redox reactions (Reaction 1) initiated by metal phase transformations. The chondritic oxygen fugacity (after homogenization) is lower than the oxygen fugacity in equilibrium with ol + opx + γ_E assemblages, causing these assemblages to undergo local reduction. The retrograde reduction reaction is manifested in ordinary chondrites by olivine Fa concentrations that decrease toward zoned taenite + kamacite particles (formed after relatively small amounts of taenite undercooling). Olivine zoning profiles near kamacite are similar to olivine zoning profiles near taenite because the activity of Fe in kamacite is identical to the activity of Fe in taenite throughout cooling. In contrast, the chondritic oxygen fugacity is higher than the oxygen fugacity in equilibrium with ol + opx + γ_M assemblages. These assemblages undergo local oxidation, as manifested by olivine Fa concentrations that increase toward zoneless plessite particles (formed after relatively large amounts of taenite undercooling).

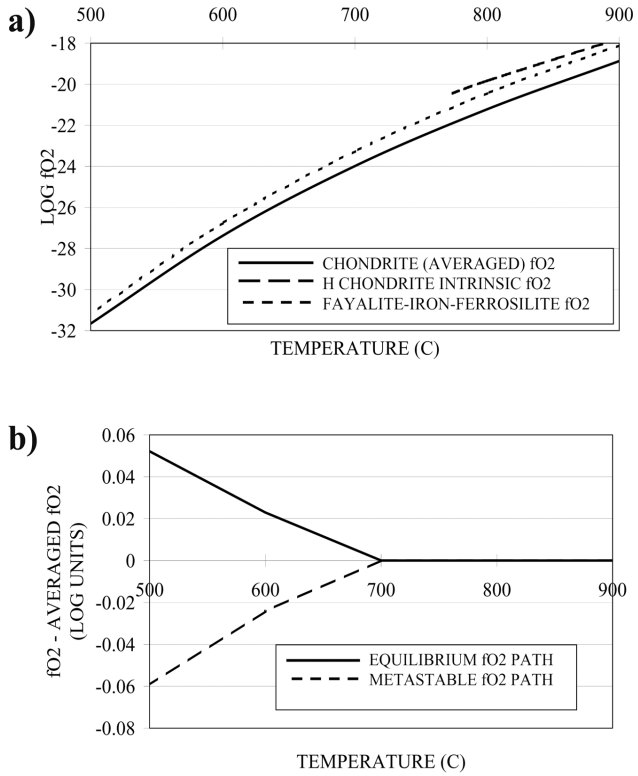

Fig. 7. a) The chondritic oxygen fugacity calculated by averaging the oxygen fugacities defined by olivine + orthopyroxene + γ_E assemblages and olivine + orthopyroxene + γ_M assemblages. The fayalite-iron-ferrosilite buffer and the intrinsic H chondrite oxygen fugacity (measured by Brett and Sato 1984) are shown for comparison. b) Oxygen fugacities defined by olivine + orthopyroxene + γ_E assemblages (equilibrium fO_2-T path) and olivine + orthopyroxene + γ_M assemblages (metastable fO_2-T path). The oxygen fugacities are shown as deviations from the chondritic (averaged) oxygen fugacity shown in Fig. 7a.

The olivine and orthopyroxene compositions shown in Fig. 8 were calculated by assuming that the metastable taenite composition (γ_M) remains constant at 10 wt% Ni throughout cooling. In reality, γ_M may become somewhat Ni-enriched during cooling as Fe becomes oxidized and incorporated into the silicates. Nonetheless, the simplified calculations are justified because the γ_M composition will remain Ni-poor relative to γ_E throughout cooling.

According to the scenario presented above, the retrograde redox reactions in ordinary chondrites were not caused by external oxygen fugacity changes. Rather, they were caused by variable amounts of taenite undercooling and were facilitated by whole-rock homogenization of the internally controlled oxygen fugacity. The redox reactions would not have occurred if every taenite particle in the chondrite had experienced the same amount of undercooling, as olivine-orthopyroxene-metal equilibria would have defined the oxygen fugacity at a single value everywhere throughout the chondrite and no disequilibrium would exist to drive changes in silicate compositions.

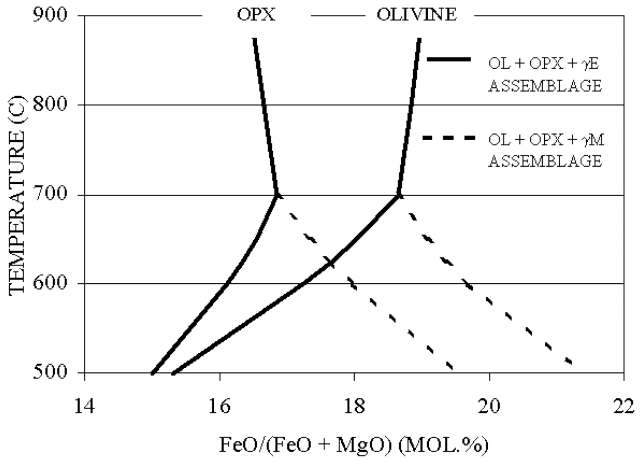

Fig. 8. The compositional evolution of olivine and orthopyroxene in ordinary chondrites during cooling. At temperatures between 900 and 700 °C, olivine Fa concentrations decrease slightly and orthopyroxene Fs concentrations increase slightly due to Fe-Mg partitioning (Reaction 2). At temperatures below 700 °C, olivine and orthopyroxene compositions undergo significant changes due to redox reactions (Reaction 1). The solid lines show the compositions of olivine and orthopyroxene that coexist with γ_E, while the broken lines show the compositions of olivine and orthopyroxene that coexist with γ_M.

Reaction Kinetics and the Absence of Measured Orthopyroxene Zoning

Olivine crystals in H5 and H6 chondrites were compositionally homogeneous at the peak metamorphic temperature, and the high temperature compositions are preserved at olivine cores. However, silicate-metal reactions during cooling produced zoning of 3–4 mol% Fa within ~30 μm of olivine-metal interfaces. The zoning developed at temperatures <700 °C, the temperature at which taenite compositions diverge along the γ_E and γ_M paths.

The average distance of diffusion in olivine can be estimated using the Einstein relation, $x = (2Dt)^{1/2}$, where x is distance, D is the olivine Fe-Mg interdiffusion coefficient, and t is time. Diffusion distances in olivine at 700, 600, and 500 °C, calculated for one million year isothermal heat treatments using interdiffusion coefficients reported by Chakraborty (1997), are 500, 100, and 10 μm, respectively. The diffusion calculations show that 30 μm long olivine Fa gradients, such as those measured in this study (Fig. 5), can indeed form at temperatures <700 °C. The relatively short diffusion profiles of ~30 μm indicate that the zoning developed at temperatures well below 700 °C. This interpretation is consistent with the expectation that the driving force responsible for the development of zoning is zero at 700 °C and becomes greater during cooling as the γ_E and γ_M compositions diverge.

The thermodynamic calculations (Fig. 8) indicate that orthopyroxene Fs concentrations should decrease toward zoned taenite + kamacite particles and increase toward zoneless plessite particles. Electron microprobe line scans across orthopyroxene crystals toward metal, however, did not reveal Fe-Mg zoning. It is possible that Fe-Mg gradients are present in orthopyroxene but are too narrow to measure with an electron microprobe. At a given temperature Fe-Mg interdiffusion in orthopyroxene is 2 orders of magnitude slower than Fe-Mg interdiffusion in olivine (Ganguly and Tazzoli 1994; Chakraborty 1997). Since diffusion distance scales with $D^{1/2}$, diffusion distances in orthopyroxene will be 1 order of magnitude smaller than those in olivine. The measured Fe-Mg diffusion distances in olivine are <30 μm (Fig. 5), suggesting that orthopyroxene Fe-Mg profiles will be <3 μm long. Such short diffusion profiles in orthopyroxene would be difficult to resolve with an electron microprobe.

Fe-Mg interdiffusion coefficients in olivine and orthopyroxene increase as oxygen fugacity increases. Since ordinary chondrites evolved under more reducing conditions than the experimental conditions used to measure the diffusion coefficients, the diffusion distances calculated in this paper may be regarded as maximum distances.

Finally, it is important to note that Fe-Mg zoning profiles can potentially develop in olivine (near Fe-Ni metal) without the formation of analogous zoning profiles in orthopyroxene. Olivine zoning profiles measured near zoned taenite + kamacite particles (decreasing Fa toward metal) are opposite from olivine zoning profiles measured near zoneless plessite particles (increasing Fa toward metal). The opposite Fe-Mg zoning profiles can be explained by exchange of Fe^{2+} and Mg^{2+} between olivine crystals via grain boundary diffusion. In this case, grain boundaries need not migrate and orthopyroxene is neither formed nor consumed. Experimental studies by Dohmen et al. (1998) demonstrate that Fe and Mg transport can occur through a gaseous phase (i.e., along grain boundaries) when the partial pressures of both species are quite low.

Implications for Ordinary Chondrites

Final Equilibration Temperatures

In H-group chondrites, the redox reactions responsible for the formation of olivine Fe-Mg zoning adjacent to metal were initiated at temperatures <700 °C (the temperature at which the metal cooled below the taenite/(taenite + kamacite) solvus). The temperature at which redox reactions apparently ceased can be estimated by comparing the olivine Fe-Mg zoning pattern measured at olivine-metal interfaces (Fig. 5) to the calculated olivine compositions shown in Fig. 8. In the chondrites we examined, olivine Fa concentrations decrease by ~2 mol% near zoned taenite + kamacite particles and increase by ~2 mol% near zoneless plessite particles (Fig. 5). The olivine composition range of 3–4 mol% Fa suggests that the redox reactions effectively ended at ~600 °C (Fig. 8). This final equilibration temperature (600 °C) is identical to the Fe-

Mg exchange closure temperature obtained for olivine-orthopyroxene pairs that are isolated from metal (compare Figs. 4 and 6).

The final equilibration temperature of 600 °C for both the redox reaction (Reaction 1) and the olivine-orthopyroxene Fe-Mg exchange reaction (Reaction 2) is below the closure temperatures recorded by orthopyroxene-diopside Fe-Mg exchange and orthopyroxene-diopside Ca exchange equilibria (820–830 °C) (Olsen and Bunch 1984). However, it is similar to olivine-spinel Fe-Mg exchange closure temperatures measured in several chondrites. For example, olivine-spinel temperatures in Bjurbole (L/LL4), Aldsworth (LL5), and Appley Bridge (LL6) are <600 °C (Johnson and Prinz 1991) and olivine-spinel temperatures in Carcote (H5) are between 570 and 720 °C (Kleinschrot and Okrusch 1999).

Metal particles in well-equilibrated H-group chondrites have bulk compositions of ~10 wt% Ni, and consequently cooled into the two-phase taenite + kamacite field at ~700 °C (Fig. 1a). This temperature was sufficiently high to allow detectable progress of silicate-metal reaction during subsequent cooling. In contrast, L and LL chondrites have whole-rock metal compositions of 15–30 wt% Ni and cooled into the taenite + kamacite field at temperatures <600 °C (Fig. 1a). The present study was limited to the examination of H chondrites (owing to the high density of silicate-metal interfaces), but the authors suspect that relatively sluggish diffusion rates at temperatures <600 °C may have limited the importance of retrograde silicate-metal reactions in L and LL chondrites.

Interpretation of "Anomalous" Olivine Compositions

Random collection of olivine analyses using the electron microprobe will occasionally sample Fe-Mg diffusion profiles that developed by retrograde silicate-metal reactions. Even olivine crystals that do not appear contiguous with metal in the plane of sectioning may be compositionally zoned due to the complex geometries of olivine-metal interfaces.

Clearly, any interpretation of olivine compositions in highly quilibrated H chondrites should recognize the important role of retrograde silicate-metal reactions. In one relevant study, Rubin (1990) reported olivine composition histograms for several H5 and H6 chondrites. In several of the chondrites, a few olivine analyses vary by up to ~2 mol% Fa from the host chondrite's mean olivine composition (see Fig. 7.7.2 in Rubin 1990). Although these chondrites lack obvious brecciation textures such as angular clasts or light-dark structures, Kallemeyn et al. (1989) and Rubin (1990) proposed that the anomalous olivine compositions represent aberrant crystals that were incorporated into the host chondrite after cooling from the peak metamorphic temperature. The same authors suggested that these post-metamorphic fragmental breccias were cemented by shock lithification at relatively low ambient temperatures (i.e., low lithification temperatures prevented the aberrant olivine crystals from equilibrating with other crystals). We do not dispute the interpretations of Kalleymen et al. (1989) and Rubin (1990), but we wish to emphasize that small amounts of olivine Fe-Mg zoning are an expected consequence of retrograde silicate-metal reaction. In fact, the existence of olivine Fe-Mg zoning adjacent to metal provides strong evidence that the silicate and metallic minerals evolved in situ during cooling from the peak metamorphic temperature.

Acknowledgments–We are grateful for constructive reviews by E. Scott, N. Chabot, and especially J. Ganguly. This work was supported by NASA grants NNG005GK84G (J. I. Goldstein) and NAG5-13226 (M. I. Petaev).

Editorial Handling—Dr. Edward Scott

REFERENCES

Berman R. G. and Aranovich L. Y. 1996. Optimized standard state and solution properties of minerals: Model calibration for olivine, orthopyroxene, cordierite, garnet, and ilmenite in the system FeO-MgO-CaO-Al_2O_3-TiO_2-SiO_2. *Contributions to Mineralogy and Petrology* 126:1–24.

Brett R. and Sato M. 1984. Intrinsic oxygen fugacity measurements on seven chondrites, a pallasite, and a tektite and the redox state of meteorite parent bodies. *Geochimica et Cosmochimica Acta* 48:111–120.

Chakraborty S. 1997. Rates and mechanisms of Fe-Mg interdiffusion in olivine at 980–1300 °C. *Journal of Geophysical Research* 102: 12,317–12,331.

Chase M. W. 1998. *NIST-JANAF thermochemical tables,* 4th ed. Journal of Physical and Chemical Reference, Monograph 9. 1951 p.

Craig H. 1964. Petrological and compositional relationships in meteorites. In *Isotopic and cosmic chemistry*, edited by Craig H., Miller S. L., and Wasserburg G. Amsterdam: North-Holland. pp. 401–451.

Dodd R. T. 1981. *Meteorites: A petrologic-chemical synthesis*. Cambridge: Cambridge University Press. 368 p.

Dohmen R., Chakraborty S., Palme H., and Rammensee W. 1998. Solid-solid reactions mediated by a gas phase: An experimental study of reaction progress and the role of surfaces in the system olivine + iron metal. *American Mineralogist* 83:970–984.

Ganguly J. and Saxena S. J. 1987. *Mixtures and mineral reactions*. New York: Springer-Verlag. 291 p.

Ganguly J. and Tazzoli V. 1994. Fe^{2+}-Mg interdiffusion in orthopyroxene: Retrieval from the data on intracrystalline exchange reaction. *American Mineralogist* 79:930–937.

Goldstein J. I., Newbury D. E., Echlin P., Joy D. C., Romig A. D., Lyman C., Fiori C., and Lifshin E. 1992. *Scanning electron microscopy and X-ray microanalysis*. New York: Plenum Press. 820 p.

Hsieh K., Vlack K. C., and Chang Y. A. 1987. The Fe-Ni-S system: A thermodynamic analysis of the phase equilibria and calculation of the phase diagram from 1173 to 1623 K. *High Temperature Science* 23:17–38.

Johnson C. A. and Prinz M. 1991. Chromite and olivine in type II chondrules in carbonaceous and ordinary chondrites: Implications for thermal histories and group differences. *Geochimica et Cosmochimica Acta* 55:893–904.

Kallemeyn G. W., Rubin A. E., Wang D., and Wasson J. T. 1989. Ordinary chondrites: Bulk compositions, classification, lithophile-element fractionations, and composition-petrographic type relationships. *Geochimica et Cosmochimica Acta* 53:2747–2767.

Keil K. and Fredrickson K. 1964. The iron, magnesium, and calcium distribution in coexisting olivines and rhombic pyroxenes in chondrites. *Journal of Geophysical Research* 64: 3487–3515.

Kleinschrot D. and Okrusch M. 1999. Mineralogy, petrography, and thermometry of the H5 chondrite Carcote, Chile. *Meteoritics & Planetary Science* 34:795–802.

Larimer J. W. 1968. Experimental studies on the system Fe-MgO-SiO_2-O_2 and their bearing on the petrology of chondritic meteorites. *Geochimica et Cosmochimica Acta* 32: 1187–1207.

McSween H. Y., Jr., and Labotka T. C. 1993. Oxidation during metamorphism of the ordinary chondrites. *Geochimica et Cosmochimica Acta* 57:1105–1114.

Miyamoto M. 1997. Chemical zoning of olivine in several pallasites. *Journal of Geophysical Research* 102:21,613–21,618.

Miyamoto M., McKay D. S., McKay G. A., and Duke M. B. 1986. Chemical zoning and homogenization of olivines in ordinary chondrites and implications for thermal histories of chondrules. *Journal of Geophysical Research* 91:12,804–12,816.

Mueller R. F. 1963. A comparison of oxidative equilibria in meteorites and terrestrial rocks. *Geochimica et Cosmochimica Acta* 27:273–287.

Mueller R. F. 1964. Phase equilibria and the crystallization of chondritic meteorites. *Geochimica et Cosmochimica Acta* 28: 189–207.

Mueller R. F. and Olsen E. J. 1967. The olivine, pyroxene, and metal content of chondritic meteorites as a consequence of Prior's rule. *Mineralogical Magazine* 36:311–318.

Olsen E. J. and Bunch T. E. 1984. Equilibration temperatures of ordinary chondrites: A new evaluation. *Geochimica et Cosmochimica Acta* 48:1363–1365.

Pellas P. and Storzer D. 1981. ^{244}Pu fission track thermometry and its application to stony meteorites. *Proceedings of the Royal Society of London A* 374:253–270.

Prior G. T. 1916. On the genetic relationship and classification of meteorites. *Mineralogical Magazine* 18:26–44.

Reisener R. J. and Goldstein J. I. 2003a. Ordinary chondrite metallography: Part 1. Fe-Ni taenite cooling experiments. *Meteoritics & Planetary Science* 38:1669–1678.

Reisener R. J. and Goldstein J. I. 2003b. Ordinary chondrite metallography: Part 2. Formation of zoned and unzoned metal particles in relatively unshocked H, L, and LL chondrites. *Meteoritics & Planetary Science* 38:1679–1696.

Rubin A. E. 1990. Kamacite and olivine in ordinary chondrites: intergroup and intragroup relationships. *Geochimica et Cosmochimica Acta* 54:1217–1232.

Sears D. W. and Axon H. J. 1975. The metal content of common chondrites (abstract). *Meteoritics* 10:486–487.

Sugiura N., Arkani-Hamed J., and Strangway D. W. 1986. Gas permeability of some Antarctic chondrites. Proceedings, 10th Symposium on Antarctic Meteorites. pp. 358–363.

Van Schmus W. R. and Koffman D. M. 1967. Equilibration temperatures of iron and magnesium in chondritic meteorites. *Science* 55:1009–1010.

Van Schmus W. R. and Wood J. A. 1967. A chemical-petrologic classification for the chondritic meteorites. *Geochimica et Cosmochimica Acta* 31:747–765.

Williams R. J. 1971. Equilibrium temperatures, pressures, and oxygen fugacities of the equilibrated ordinary chondrites. *Geochimica et Cosmochimica Acta* 35:407–411.

Willis J. and Goldstein J. I. 1983. A three-dimensional study of metal grains in equilibrated, ordinary chondrites. Proceedings, 14th Lunar and Planetary Science Conference. pp. B287–B292.

Wood J. A. 1967. Chondrites: Their metallic minerals, thermal histories, and parent planets. *Icarus* 6:1–49.

Yang C. W., Williams D. B., and Goldstein J. I. 1997. Low-temperature phase decomposition in metal from iron, stony-iron, and stony meteorites. *Geochimica et Cosmochimica Acta* 61: 2943–2956.